Agricultural and Forest Meteorology 353 (2024) 110041

Contents lists available at ScienceDirect

Agricultural and Forest Meteorology

journal homepage: www.elsevier.com/locate/agrformet

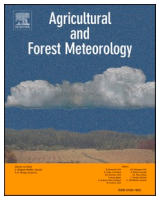

Validation of a short-range dispersion and deposition model using field-scale ammonia and methane release experiments

Christoph Häni [a,*], Albrecht Neftel [b], Christophe Flechard [c], Christof Ammann [d], Alex Valach [a], Thomas Kupper [a]

[a] School of Agricultural, Forest and Food Sciences HAFL, Bern University of Applied Sciences, Zollikofen 3052, Switzerland
[b] Neftel Research Expertise, Wohlen b. Bern, 3033, Switzerland
[c] French National Research Institute for Agriculture, Food and Environment (INRAE), 35042 Rennes CEDEX, France
[d] Climate and Agriculture Group, Agroscope Research Station, Zürich 8046, Switzerland

ARTICLE INFO

Keywords:
Backward Lagrangian stochastic
Dispersion model
Ammonia
Methane
Short range dispersion

ABSTRACT

Methods to measure gaseous emissions from spatially confined sources often rely on atmospheric dispersion models to relate downwind concentration or flux measurements to the respective emission rate. A backward Lagrangian stochastic (bLS) model was validated, which has been enhanced to incorporate surface dry deposition for trace gases for which this removal process is significant, such as ammonia (NH_3). Controlled release experiments were carried out at a grassland site with a parallel release of NH_3 and methane (CH_4) at a known release rate through a source grid with 36 critical orifices. NH_3 and CH_4 concentrations and vertical fluxes were measured downwind of the source grid and the bLS model was used to infer the release rates from the measured quantities. The median recovered fractions (ratios between the model-inferred emission rate and the actual release rate) ranged between 0.96 and 1.11 for CH_4 and between 0.32 and 0.72 for NH_3. The smaller recovered fraction of NH_3 compared to CH_4 was attributed to NH_3 dry deposition loss downwind of the source. Surface deposition velocities were inferred to account for smaller recovered fractions from experiments in which both NH_3 and CH_4 were measured in parallel. Median surface deposition velocities varied between 1.7 and 5.8 cm s^{-1} for the individual release days, which correspond to deposition velocities at a commonly used height of 2 m between 0.6 and 1.7 cm s^{-1}. Compared to literature values this is in the expected range of deposition velocities for grassland sites.

1. Introduction

Atmospheric turbulent dispersion models relate the emission of a trace gas to the respective dispersion of the emitted compound, i.e. the 3-D longitudinal, lateral and vertical spread called plume. One practical application of this kind of modeling, frequently called the "inverse dispersion method" (IDM), infers the upwind source strength from the measured average trace gas concentration at a certain downwind location in the plume. Another application links the source strength to the average vertical trace gas flux often measured by eddy covariance (EC).

The backward Lagrangian stochastic (bLS) atmospheric dispersion model introduced by Flesch et al. (2004) is frequently used to estimate emissions of trace gases like methane (CH_4) and ammonia (NH_3) from a variety of source types in the agricultural sector (Bai et al., 2014; Lavrsen Kure et al., 2018; Lemes et al., 2023; Leytem et al., 2011; McGinn et al., 2008; Shonkwiler and Ham, 2018; Sintermann et al., 2011). While such emission estimates could be done based on vertical flux (e.g., EC) measurements, most published emission estimates using the bLS model are based on concentration measurements downwind of the respective sources due to the simplicity and (relative) inexpensiveness of the concentration measurements. There are several publications available (Feitz et al., 2018; publications in Table A1 in Harper et al., 2010; Hu et al., 2016; Ro et al., 2013; Wang et al., 2014) on the experimental validation of the concentration to emission relationship estimated by the bLS model by Flesch et al. (2004). However, to our knowledge, only two publications exist on the validation of the modelled vertical flux as measured by EC (Coates et al., 2017, 2021). From the modeling perspective, the absence of validation of the modelled vertical flux does not seem critical, since the validation findings from release experiments based on concentration enhancements should be consistent with, and

* Corresponding author.
E-mail address: christoph.haeni@bfh.ch (C. Häni).

https://doi.org/10.1016/j.agrformet.2024.110041
Received 14 December 2023; Received in revised form 25 April 2024; Accepted 30 April 2024
Available online 16 May 2024

thus transferable to, vertical flux-based findings, but experimental evidence with simultaneous verification of flux and concentration is lacking.

Some validation experiments based on the release of NH_3 (Häni et al., 2018; Yang et al., 2016) have demonstrated the complication of quantifying NH_3 emissions since this highly sticky, soluble and reactive trace gas can readily adsorb upon contact with any surface. The standard model for practically inert trace gases (i.e., gases with atmospheric lifetimes orders of magnitude longer than field-scale short-range transport time scales, such as CH_4) will underestimate the total NH_3 emission from specified sources due to this temporary or permanent removal of NH_3 by dry deposition to the underlying soil and vegetation surfaces between the source and the receptor (gas sensor) location. Thus, for trace gases such as NH_3 which are prone to significant uptake on canopy and ground surfaces, modelled concentrations and fluxes will be too large with respect to the model source strength and, therefore, emissions derived from field measurements will be too small. Consequently, validations based on controlled NH_3 release provide recovered fractions that are biased low, unless dry deposition is accounted for in the dispersion model.

The controlled NH_3 release experiment by Häni et al. (2018) resulted in average recovered fractions (i.e., the ratio between the model-based estimate and the actual release rate $Q_{bLS}/Q_{release}$) between 0.69 and 0.91 depending on the location of the instrument, revealing the possible, systematic underestimation of modelled NH_3 emission rates using IDM due to dry deposition removal. Häni et al. (2018) subsequently extended the bLS model by Flesch et al. (2004) with a dry deposition algorithm, which was able to account for the missing (dry-deposited) NH_3 fraction.

In the present study, a series of controlled gas release and plume measurement experiments was conducted using a mixture of NH_3 and CH_4, where CH_4 provided the reference for a conserved trace gas without significant deposition. The objective of the release experiment was to quantify the differences in CH_4 and NH_3 recovered fractions (i.e., $Q_{bLS}/Q_{release}$) first, without considering deposition, and then attribute the apparent losses to NH_3 dry deposition between the release and measurement locations. The deposition velocity for NH_3 in the model was adjusted to yield the same recovered fractions as observed for CH_4. We further validated the model for simultaneous concentration measurements at various distances downwind of the source and for eddy covariance flux measurements.

2. Materials and method

2.1. Controlled release experiments

A total of 11 artificial release experiments were carried out between Nov. 2016 and Apr. 2017 at the Agroscope research site in Posieux, Switzerland (46.76783 N, 7.10753 E; altitude 640 m a.s.l.). The experimental site extended to a 60 m by 60 m square situated in the center of a 4 ha pasture. There were two farms located approx. 100 m north and southeast of the site. The upwind direction, up to 500 m southwest of the site, was dominated by gently sloped pastureland. The average grass canopy height at the experimental site was 6 cm (CH4-I to Mix-V) and 18 cm (Mix-VI to Mix-IX), respectively.

Methane and ammonia were released from gas standard cylinders at a controlled flow rate through a grid of 36 critical orifices (100 μm diameter, stainless steel, Lenox Laser Inc., Glen Arm, MD, USA) representing an approximately circular source area with a diameter of 20 m. The artificial source is described in more detail in Häni et al. (2018). During the first two experiments, i.e., CH4-I and CH4-II, pure (100 %) CH_4 was released, whereas for the following 9 experiments, i.e., Mix I-IX, a gas mixture of 95 % CH_4 and 5 % NH_3 (±2 % rel., Carbagas, Bern, Switzerland) was used (Table 1). The flow rate was controlled using a mass flow controller (red-y smart controller, CH_4, max. flow at 30 L_n min^{-1}, Voegtlin Instruments GmbH, Aesch, Switzerland) at a release rate between 20 and 25 L_n min^{-1}, with a lower release rate of 15 L_n min^{-1} for a duration of approx. 1 h at the beginning of CH4-I, which resulted in total (usable) release times between 1 h 10 min and 2 h per gas cylinder. Prior to the release phases Mix I-IX, the source grid was flushed with the gas mixture at a low flow rate for approx. 30 min to reduce the effect of NH_3 absorption inside the grid during the actual release period.

The trace gas concentrations were measured at distances of 0, 15 and 30 m downwind and approx. 15 m upwind of the source center (Fig. 1). For line-integrated measurements, these numbers represent the distance between the source center and the center of the optical path. The measurements consisted of path-averaged concentration measurements using open-path sensors (Section 2.2) and point measurements at 30 m downwind using closed-path sensors (Section 2.3). The path-averaged concentrations were measured over path lengths of 35 to 40 m. The measurement heights were 1.3 m a.g.l. at all measurement locations with additional measurement heights of 0.6 m a.g.l. (NH_3 and CH_4), 2.1 m a.g.l. (NH_3 only) and 1.8 m a.g.l. (closed-path measurements) at 30 m distance from the source.

2.2. Line-integrated concentration measurements

2.2.1. GasFinder instruments for CH_4 concentration measurements

Line-integrated concentrations of CH_4 were measured using open-path tunable diode laser (centered around 1654 nm) spectrometers (GasFinder2[1] and GasFinder3 (GF); Boreal Laser Inc., Edmonton, Canada). The GF instruments measure the path-averaged CH_4 concentration between a laser source/receptor and a reflector based on light absorption of the infrared laser beam. They were cross-calibrated twice on-site to the quantum cascade laser (QCL) instrument (Section 2.3). Due to possible drifts in the concentration measurements provided by the GF instruments (Häni et al., 2021) the measured concentrations were aligned to match the QCL concentrations prior to and after each release experiment. It was ensured that the measurement quality constraints as indicated by Boreal Laser Inc. (2016) were met during the releases. The measured, path-integrated CH_4 concentration in ppm·m (parts per million meter) was divided by the single-path length and corrected using on-site measurements of air temperature and pressure with the temperature and pressure correction functions provided by the manufacturer to obtain the concentration in ppm, which was further converted to units of mg m^{-3}. The single-path lengths varied between 35 and 40 m (distance between laser and reflector), resulting in a measurement precision of approx. 0.1 mg m^{-3} or 0.15 ppm (Häni et al., 2021).

Despite the concerns in Häni et al. (2021), the downwind measurements of CH_4 with the GF instruments seemed to be sufficiently stable for the time of the individual releases and, further, were most of the time substantially higher than the background concentration including the indicated measurement precision. However, the measured inflow concentrations during the release experiments CH4-I to Mix-III were discarded due to the limited quality (concentration drifts) of the concentration measurements at background concentrations as observed by Häni et al. (2021). Although these instrument-related drifts were not severe (approximately 0.1 mg m^{-3}), the CH_4 inflow measurement added additional uncertainty to the concentration differences and, consequently, the usage of an additional CH_4 measurement downwind of the source was preferred over an actual inflow measurement during later release experiments (i.e., Mix-IV to Mix-IX). Since there were no CH_4 sources in the upwind proximity and the lowest 5 % of the high-frequency measurements from the point measurements (QCL; Section 2.3) were observed to be stable at background value during the releases, the background CH_4 concentrations were linearly interpolated from the background concentration measurements directly before and after each release for each downwind GF separately to remove potential

[1] GasFinder2 instruments were used during the 2016 release experiments (Table 1).

Table 1
Individual release experiments between Nov. 2016 and Apr. 2017. x_m: distance in meter between source center and center of measurement path. inflow: measurement location approx. 15 m upwind of the source center. z_m: average measurement height in meters above ground level. Line-integrated measurement: path-averaged concentration measurement using GasFinder2 (GF2) and GasFinder3 (GF3) instruments for CH_4 and miniDOAS (MD) instruments for NH_3 concentration measurement over a path length of approx. 40 m. Point meas.: closed-path, point measurements of CH_4 and NH_3 using a Quantum Cascade Laser Spectrometer (QCL) and a Dual-Channel Thermal Converter (DTC), respectively.

Release	Date	Start	Stop	Release Duration	Released Gas*	Flowrate	Release rate		Line-integrated measurements							Point meas.
							CH_4	NH_3	x_m;	0	15	30			upwind	30
		CET/CEST				L_n min^{-1}	mg s^{-1}	mg s^{-1}	z_m;	1.3	1.3	0.6	1.3	2.1	1.3	1.8
CH4-I	04.11.16	13:00	15:10	2h00	CH4	15 / 20**	179 / 239	–			**GF2**		**GF2**		**GF2**	**QCL**
CH4-II	08.11.16	15:00	16:35	1h35	CH4	20	239	–			**GF2**		**GF2**		**GF2**	**QCL**
Mix-I	17.11.16	09:09	10:45	1h10	Mix	20	227	12.6			**GF2 / MD**	**MD**	**GF2 / MD**		**GF2 / MD**	**QCL**
Mix-II	17.11.16	11:36	13:09	1h20	Mix	24	272	15.2			**GF2 / MD**	**MD**	**GF2 / MD**		**GF2 / MD**	**QCL**
Mix-III	17.11.16	13:41	15:26	1h30	Mix	23	261	14.5			**GF2 / MD**	**MD**	**GF2 / MD**		**GF2 / MD**	**QCL**
Mix-IV	17.03.17	15:00	16:39	1h30	Mix	20	227	12.6		**GF3 / MD**		**GF3 / MD**	**GF3 / MD**		**MD**	**QCL / DTC**
Mix-V	21.03.17	10:53	12:45	1h50	Mix	20	227	12.6		**GF3 / MD**		**GF3 / MD**	**GF3 / MD**		**MD**	**QCL / DTC**
Mix-VI	10.04.17	12:00	14:00	2h00	Mix	20	227	12.6		**GF3 / MD**		**GF3 / MD**	**GF3 / MD**	**MD**	**MD**	**QCL / DTC**
Mix-VII	10.04.17	14:25	15:20	0h40	Mix	25	283	15.8		**GF3 / MD**		**GF3 / MD**	**GF3 / MD**	**MD**	**MD**	**QCL / DTC**
Mix-VIII	13.04.17	06:54	07:40	0h40	Mix	20	227	12.6		**GF3 / MD**		**GF3 / MD**	**GF3 / MD**	**MD**	**MD**	**QCL / DTC**
Mix-IX	13.04.17	07:47	10:25	1h40	Mix	20	227	12.6		**GF3 / MD**		**GF3 / MD**	**GF3 / MD**	**MD**	**MD**	**QCL / DTC**

* CH4: pure (100 %) CH_4; Mix: mix of 95 % CH_4 and 5 % NH_3.
** approx. 1 h with 15 L_n min^{-1} and 1 h with 20 L_n min^{-1}.

instrument drifts. Subtraction of the interpolated background concentrations provided the concentration enhancements related to the controlled release of CH_4.

2.2.2. *miniDOAS instruments for NH_3 concentration measurements*

The measurements of line-integrated NH_3 concentrations were made using open-path miniDOAS spectrometers (Sintermann et al., 2016). The miniDOAS instrument measures light absorption from gaseous NH_3, NO and SO_2 in the UV range between 200 and 230 nm. The nominal precision of the instrument is 0.2 μg m^{-3} or 1.4 % of the measured concentration. During the release, the intensity level of the received light was kept close to the maximum to maintain a high sensitivity to concentration changes and ensure high quality measurements.

For the NH_3 background concentrations, the incoming NH_3 concentration measured upwind of the source using a miniDOAS instrument was subtracted from the downwind concentration measurements to obtain the source-related NH_3 concentration increases. Incoming NH_3 concentration peaks did not occur during the release periods.

2.3. *Point concentration measurements*

In addition to the line-integrated measurements, point measurements of CH_4 and NH_3 concentrations were performed using closed-path measurement instruments. Methane was measured using a QCL (QC-TILDAS, Aerodyne Research Inc.) during all releases, whereas NH_3 was measured for the releases Mix-IV to Mix-IX with a dual-channel chemiluminescence NO detector (CLD899, EcoPhysics, Dürnten, Switzerland) in combination with a dual-channel thermal converter (DTC; Ammann et al., 2019). The NOy channel measures the sum of all oxidized nitrogenous compounds and the Nr channel the sum of all oxidized and reduced compounds (Ammann et al., 2012). Thus, the difference between the two channels corresponds to the sum of reduced compounds (NHx). In agricultural areas and especially in the present release experiment, the NHx signal is strongly dominated by NH_3 with negligible contributions of particulate NH_4^+.

Both the QCL and the DTC, measured with fast response at a temporal resolution of 10 Hz. The high-resolution data was processed to provide average concentrations as well as average vertical fluxes using the eddy covariance (EC) method (see Section 2.4).

2.4. *Vertical turbulent flux measurements*

Vertical fluxes of CH_4 and NH_3 were calculated from the measurements of the closed-path instruments (Section 2.3) using the eddy covariance (EC) method. The ultrasonic anemometer (HS-50, Gill Instruments, Lymington, UK) was located within 20 cm of the sampling line inlets at 1.8 m a.g.l. The fluxes were calculated for each individual 10-minute interval, based on the covariance between the 10 Hz measurements of the gas concentration and the vertical wind velocity (w) using the programming language R (https://www.r-project.org/). Prior to the evaluation, the wind velocity vectors were double rotated into the average wind direction and both the vertical velocity and concentration measurements were de-spiked and detrended; the vertical velocity measurements were detrended linearly and the concentration measurements by subtracting the 5-minute moving average. The averaging of the flux based on 10-minute intervals in this study is shorter compared to common flux measurements by EC, which are typically integrated over 30 min or longer. However, evaluation of the flux based on 30-minute intervals with a linear detrending of both the concentration, and the velocity measurements, showed that the contribution from the lowest frequencies is negligible in the given setup.

The lag times between the concentration and wind measurements were derived from maximization of the corresponding covariances of the vertical velocity and concentration fluctuations. They were found to be around 6 s for CH_4 and around 9 s for NH_3 flux estimates (Supplement-1 Fig. 1). The high-frequency damping of the concentration fluxes was

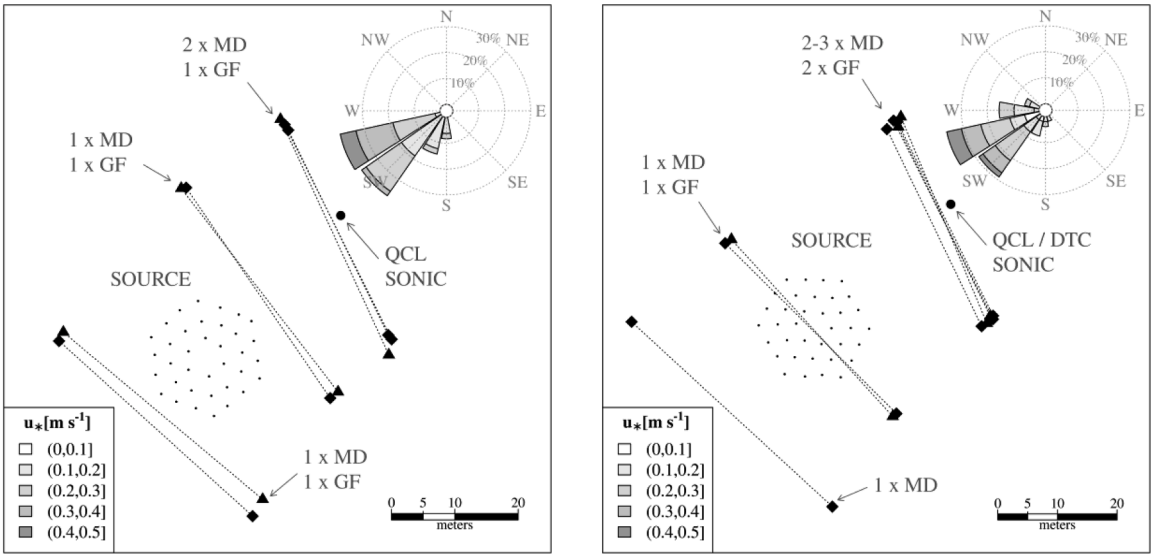

Fig. 1. Setup of artificial source and measurement instruments during releases in 2016 (left) and 2017 (right); dotted lines indicate the optical paths of line-integrated measurements. SOURCE: the source grid is indicated as 36 dots representing the positions of the orifices. SONIC: 3D sonic anemometer, measurement height at 1.8 m a.g.l. Line-integrated concentration measurements were made using GasFinder (GF) instruments for CH_4 and miniDOAS (MD) instruments for NH_3; Closed-path point concentration measurements were made using a Quantum Cascade Laser (QCL) spectrometer for CH_4 and a Dual-Channel Thermal Converter (DTC) for NH_3. Distances from the center of the source to the center of the sensors are approx. 0 m, 15 m and 30 m. The setup change between 2016 and 2017 included a relocation of the sensors at 15 m distance to 0 m distance from the source as well as a relocation of the upwind GF instrument to a CH_4 measurement at 30 m distance from the source at a low measurement height. The instrument measurement heights are given in Table 1.

estimated from linearly (robust) fitting the corresponding cumulative co-spectra (ogive) to the ogive of the vertical heat flux (Ammann et al., 2006) in the frequency range between 0.05 and 0.5 Hz (Supplement-1 Figs. 2 and 3). The damping effect was estimated to reduce flux measurements by around 20 % (CH_4) and 40 % (NH_3) on average. Estimating the high-frequency damping in the measured NH_3 flux is challenging. Depending on the measurement setup the damping might also affect comparably low frequencies (Wintjen et al., 2020) and classical damping estimation methods may be off. Due to the short interval duration of 10 min, it was necessary to set the upper frequency limit for ogive fitting relatively high (0.5 Hz), where the high-frequency damping may still significantly affect the co-spectra, and the resulting estimate of the damping may therefore be too low.

Within the relevant wind directions, background fluxes of CH_4 and NH_3 were not distinguishable from zero and were, therefore, assumed to be negligible during the release experiments.

NH_3 fluxes were neither corrected for H2O interference (Ammann et al., 2012) nor was a WPL correction applied, since these corrections were estimated to be small (< 1 %) compared to the observed flux magnitudes.

Because the source covered only a small fraction of the EC flux footprint, the vertical fluxes were footprint corrected, i.e., corrected for their footprint "coverage" using the dispersion factors estimated by the atmospheric dispersion model as described in the following section.

2.5. Dispersion model

The backward Lagrangian stochastic (bLS) model was used as described in Flesch et al. (1995), Flesch (1996) and Flesch et al. (2004). The model has been extended with a dry deposition algorithm and is available as R package *bLSmodelR* at https://github.com/ChHaeni/bLSmodelR. The quantification of dry deposition to a theoretical, non-emitting surface is based on a surface deposition velocity v_d^*, which represents the inverse of the transfer resistance between the trajectory touchdown (TD) at the surface of the model domain and the notional height of uptake at the canopy and soil surfaces (Häni et al., 2018). For a thorough description of the model dry deposition calculation we refer to Häni et al. (2018).

The model calculates for each sensor position, measurement interval and spatially distinct ground source the dispersion factors for concentration (D_{conc} with units s m^{-1}) and vertical flux (D_{flux}; unitless), i.e., the ratios of the expected enhancements of the average concentration C, and the average vertical flux $\overline{w'C'}$ at the sensor location, to the average emission flux. Dividing the measured vertical flux by the dispersion factor D_{flux} (without the inclusion of deposition) is commonly denoted footprint correction of the flux. Details on the calculation of the dispersion factors is given in Supplement-1 Section 2.

The model-based estimate of the source strength Q_{bLS} is calculated from measured quantities, either from the concentration enhancement or from the turbulent flux, providing two independent assessments, such as:

$$Q_{bLS} = \begin{cases} A\cdot\left(\overline{C}_{meas} - \overline{C}_{bgd}\right)/D_{conc} \\ A\cdot\left(\overline{w'C'}_{meas} - \overline{w'C'}_{bgd}\right)/D_{flux} \end{cases} \quad (1)$$

Where the overbar denotes the temporal average over the respective interval duration, $\overline{w'C'}$ represents the vertical turbulent flux, and C the concentration of the trace gas. The subscripts *meas* and *bgd* represent the quantities measured at the sensor location with the source emission included (*meas*) and with the source emission notionally excluded (*bgd*). In the case of concentrations, the latter is often approximated by measurements upwind of the source as has been done for the NH_3 measurements (Section 2.2.2), or, the value for $\overline{C}_{bgd}$ is interpolated between concentrations measured at different points in time (as described in Section 2.2.1 for the CH_4 measurements). In the case of vertical flux, the background flux was negligibly small for both NH_3 and CH_4 fluxes and could be set to zero (Section 2.4).

Line-integrated sensors were discretized into approx. 80 averaged points distributed every 0.5 m along each sensor's optical path. The calculation was performed based on $5{\cdot}10^6$ trajectories for point sensors and 10^6 trajectories for each of the discretization points in the case of line-integrated sensors.

The source grid was modelled as 36 circular areas with radii of 5 cm representing the 36 orifices. The 5 cm radii were large enough to allow

sufficient touchdowns inside the source area, but still small enough to represent the deposition of NH_3 in the immediate vicinity surrounding the orifices. In the case of the profile model calculations presented in Fig. 3 in Section 3.4, the source was modelled as a circular area with a radius of 10 m.

In addition to the geometry of the source and sensors, the model input required the following parameters derived from high-frequency ultrasonic anemometer data (Section 2.4): the friction velocity (u_*), the Obukhov length (L), the roughness length (z_0), and the standard deviations of the wind velocity components scaled to the friction velocity (σ_u/u_*, σ_v/u_* and σ_w/u_*) as well as their corresponding measurement height. z_0 was estimated as described in Häni et al. (2018), whereby the equation of the vertical profile of the average wind speed is solved given the average measured wind speed at the height of the ultrasonic anemometer and the calculated values of u_* and L.

2.6. Data quality assessment

Estimates of Q_{bLS} were filtered to fulfill the model assumptions of atmospheric turbulence and stationarity, as well as to obtain enough touchdowns within the source area and to be based on significant concentration and flux enhancements above the background. From the total number of 789 data from 97 intervals, 576 data (89 intervals) passed all quality assessments and were included in the final analysis.

Specific quality criteria for valid 10-min data were as follows:

- the data-based estimate of z_0 was smaller than the canopy height z_c, i.e., $z_0 < z_c$,
- the standard deviation of the cross-wind component (σ_v) normalized by u_* was smaller than 8, i.e., $\sigma_v/u_* < 8$,
- the absolute value of the inverse of L was smaller than 1, i.e., $|1/L| < 1$,
- the duration of the gas release was more than 50 % of the interval duration, i.e., ≥ 5 min,
- and more than 500 (point sensor) or 5000 (line sensor) touchdowns per m^2 were located inside the source area (around 0.01 – 0.5 % of the released trajectories).

Finally, data where the lower bound of the 95 % confidence interval (95 %-CI) of the recovered fraction (Section 2.7) was below 0 were removed. These data reflected individual estimates which contained a large uncertainty either due to a weak source-sensor signal (in the concentration or vertical flux) or due to uncertainty in the modelled dispersion factor.

The 95 %-CI was derived from a Monte Carlo simulation where the following individual uncertainties were assumed: 0.01 mg m^{-3}, 0.025 mg m^{-3} and 0.1 mg m^{-3} for point, line-integrated and background measurements of CH_4 concentrations; 0.1 µg m^{-3} for point measurements and standard errors that were obtained from the raw data evaluation for line-integrated NH_3 concentrations; 10 % for vertical flux measurements; 5 % for the source release strength; and both a relative uncertainty of 10 % as well as the model-estimated standard error for the bLS dispersion factors.

2.7. Calculation of recovered fractions

The fraction of the released trace gases recovered by the bLS model (ξ) was given by the ratio between the source strength Q_{bLS} inferred from concentration (or flux) measurements and dispersion modeling (Section 2.5) and the actual released amount of trace gas at the source $Q_{release}$, set by the mass flow controller:

$$\xi = Q_{bLS}/Q_{release} \quad (2)$$

Note that, due to the relationship given in Eq. (1), ξ is equivalent to the ratio between the measured concentration enhancement (or vertical flux enhancement) and the corresponding modelled enhancement based on $Q_{release}$.

A CH_4-normalized recovered fraction for NH_3 ($\xi_{NH3/CH4}$), i.e., the ratio of the NH_3 recovered fraction (ξ_{NH3}) to the corresponding CH_4 recovered fraction (ξ_{CH4}) derived from parallel measurements at the same location (equal distance to source and equal measurement height) and based on the same measurement type (EC flux, line-integrated concentration or point concentration measurements), was calculated as:

$$\xi_{NH3/CH4} = \xi_{NH3} \Big/ \xi_{CH4} \quad (3)$$

The two instruments that measured NH_3 and CH_4 in parallel were located closely next to each other and the bLS dispersion factor without correction for deposition loss (i.e., D^0_{conc} or D^0_{flux}) can be assumed equal for the two trace gases for the same measurement interval and, therefore, $\xi_{NH3/CH4}$ is almost independent of biases in the modelled dispersion. The superscript 0 (e.g., ξ^0_{NH3}) indicates that dry deposition loss is not accounted for. This metric is used throughout the manuscript to explicitly indicate NH_3 related quantities derived without deposition correction (i.e., $v_d^* = 0$). For CH_4 with generally negligible deposition, ξ_{CH4} and ξ^0_{CH4} are assumed to be identical.

2.8. Estimation of dry deposition velocity for ammonia

The dry deposition modeling is based on the assumptions that, within each interval, the surface is perfectly homogeneous with a constant v_d^* outside the specified source areas and zero deposition inside, i.e., in the case of a source consisting of 36 small circular areas representing the artificial source, NH_3 is deposited in between individual orifices. Furthermore, the model acknowledges only one source of modelled trace gas in the model domain – the artificial tracer release system – and the inflowing background concentrations and fluxes equal zero in all model calculations, i.e., the modelled concentrations and vertical fluxes represent "isolated" enhancements above background levels. Consequently, any modelled deposition originates only from the emission of this source, e.g., deposition of background NH_3 is not included in any of the presented profiles in Section 3.4.

In the presented analysis, the deposition algorithm was run for each 10-min interval for a range of v_d^* values and the corresponding CH_4-normalized recovered fractions $\xi_{NH3/CH4}$ were estimated. With this set of $\xi_{NH3/CH4}$ values, the best fitting deposition velocity $\tilde{v}_d^*$ was estimated by linear interpolation such that ξ_{NH3} equaled ξ_{CH4} (i.e., $\xi_{NH3/CH4} = 1$).

The $\tilde{v}_d^*$ values were additionally converted to corresponding deposition velocities referenced at 2 m height above ground ($\tilde{v}_d$; Supplement-1 Section 3) to provide better comparability to literature values.

3. Results and discussion

3.1. Meteorological conditions and concentration enhancement during the release

Release periods were chosen to cover a substantial variation in meteorological, turbulence and stability conditions and in the resulting release-induced concentration and vertical flux enhancements over the 11 release experiments (Supplement-1 Fig. 4 to 10, and Table of final data set in Supplement-2). Variations in atmospheric conditions included u_* values ranging between 0.08 and 0.49 m s^{-1} and atmospheric stabilities mainly in the neutral and unstable range with few measurements also in the stable range. In the final set of valid results, the concentration enhancements ranged from 0.2 to 3.9 mg CH_4 m^{-3} and from 3.4 to 143.7 µg NH_3 m^{-3} which reflected the wide range of weak to moderate emission plumes encountered in agricultural emission measurements (see e.g. supplementary data of Bühler et al. (2021) and Valach et al. (2023)). Raw EC fluxes ranged from 31 to 172 µg CH_4 m^{-2} s^{-1} and from 0.28 to 4.59 µg NH_3 m^{-2} s^{-1}, respectively.

3.2. Recovered fractions without considering deposition

3.2.1. CH_4

Median recovered fractions for the CH_4 release ξ_{CH4} ranged between 0.96 and 1.11 (Table 2). These values close to 1 indicate an accurate measurement and modeling setup for CH_4 which behaves as a relatively inert tracer over short distances of tens of meters. The lower and upper bounds of the 95 %-CI[2] indicate a model uncertainty (precision) for single interval estimates of roughly 20 to 35 % for line-integrated measurements that are positioned well inside the trace gas plume (i.e., at distances 15 m and 30 m). This was better than recent estimates of the model uncertainty based on dairy housing emission measurements as high as 60 % (Bühler et al., 2021), and agreed well with uncertainty estimates based on previous trace gas releases with 20 to 40 % (Häni et al., 2018) and 20 to 60 % (Table A1 in Harper et al., 2010). Results from point concentration measurements and the line-averaged measurements above the source showed a larger uncertainty around 60 %, whereas the flux measurement based results were characterized by an even higher value of uncertainty around 130 %. In general, larger deviations from $\xi_{CH4} = 1$ could be related to intervals where the footprint coverage of the source in the concentration or the vertical flux measurement was poor. The low footprint coverage over the source results in smaller levels of both measured concentration (or flux) enhancement and modelled dispersion factor with higher relative levels of uncertainties. In the case of measurements at the plume edge, small deviations in the wind direction result in large changes of the modelled dispersion factor due to the steep, local concentration or flux gradients at the plume edge. This is visible, e.g., in the point measurement example in Fig. 2, where emissions in the northeast corner of the source have an approx. 350 times higher contribution to the measured concentration compared to emissions in the southwest corner of the source. A similar sensitivity is also visible for the flux measurement (Fig. 2, left). However, the line-integrated measurement is much less sensitive to this geometry effect (Fig. 2, right). By requiring that acceptable model results contained a sufficient number of touchdowns inside the source area (Section 2.6), such unfavorable measurements at the edge of the plume were to a large part removed for this study. As a consequence, the percentage of valid intervals included from the total available intervals is lower in the case of the point concentration and flux measurements compared to the line-integrated measurements (Table 2).

3.2.2. NH_3

Systematically lower recovered fractions were found for NH_3 with median ξ^0_{NH3} values ranging between 0.32 and 0.72 (Table 2). It can be assumed that there was no significant difference in the emission estimations compared to CH_4 which could be introduced by either the setup, the modeling, or the measurements. Therefore, the lower recovered fractions for NH_3 indicate removal of NH_3 between the release (at the orifice) and the downwind measurement locations. There are four possible pathways to account for gaseous NH_3 removal between the source and the measurement site: 1) homogeneous gas phase chemical reaction; 2) heterogenous interaction with particulate matter; 3) precipitation scavenging and subsequent wet deposition; 4) surface dry deposition. Removal pathways 1) and 2), i.e. chemical reaction and particulate partitioning, are expected to have altered the NH_3 fluxes and concentrations only marginally over the very short transport distances and times in our setup (Loubet et al., 2009; Nemitz et al., 2009). Because precipitation did not occur during any of the 'Mix' releases, wet deposition can be excluded as a removal pathway and, therefore, it can be concluded that the removal of NH_3 was overwhelmingly due to dry deposition.

Across all the release experiments, the estimated NH_3 recovered fractions generally showed a wider variation in relative terms to their median values compared to the CH_4 results. This does not necessarily reflect a larger uncertainty in the NH_3 recovered fraction estimation, but rather the additional variation in the recovered fractions due to varying meteorological and surface conditions (i.e., changes in wind direction, friction velocity, surface wetness, etc.), which change the magnitude of the dry deposition removal and/or the source location in the footprint geometry (and thus the relative effect of the deposition removal), therefore resulting in different concentration and flux reductions due to dry deposition.

3.3. Inferring NH_3 dry deposition velocities from recovered fractions

The median $\widetilde{v}^*_d$ over all concentration measurements within a single experiment varied across the different experiments between 1.7 and 5.8 cm s^{-1}, with comparably high variation in the individual estimates of $\widetilde{v}^*_d$ themselves (robust standard deviations vary from 0.7 to 3.1 cm s^{-1}, equaling 35 % to 60 % of the corresponding median values) (Table 3).

Values of the deposition velocity extrapolated to a reference height of 2 m ($\widetilde{v}_d$) ranged from 0.6 to 1.7 cm s^{-1} and compared well to the values published by Schrader and Brümmer (2014) who present an average deposition velocity of 0.9 cm s^{-1} (values range from 0.1 to 1.8 cm s^{-1}) for semi-natural sites (including grassland sites).

There was no evidence of NH_3 saturation at the absorbing surfaces, which might have been observed as a decrease in measurement-derived $\widetilde{v}^*_d$ over time within the same experiment. Also surprisingly, we did not observe a dependence of dry deposition on air temperature or relative humidity, which would be expected from current mechanistic understanding of non-stomatal dry deposition processes (Supplement-1 Fig. 21). This might give evidence for the complexity of the actual dry deposition mechanism: ammonia dry deposition depends on the actual surface-level NH_3 concentration, which is controlled by the underlying abundance of volatilizable ammonium (NH_4^+) in solution in soil and plants, and in free water (rain, dew) on plant and leaf surfaces. The thermodynamics regulating the NH_3/NH_4^+ equilibrium are controlled by water content (dilution), temperature (Henry constant) and pH (protonation constant) at the surface; foliar absorption of NH_3 also depends on solar radiation, which controls stomatal opening.

It was assumed that $\widetilde{v}^*_d$ is spatially homogeneous and constant in time for the duration of a single release experiment (approx. 2 h, see Table 1) and the observed variability in $\widetilde{v}^*_d$ within each experiment results from measurement and dispersion modeling errors besides the simplification of the deposition pathway in the model. Thus, the likeliest estimate for $\widetilde{v}^*_d$ within each experiment was provided by the median value over all (line-integrated and point) concentration measurements within that experiment (Table 3: *all conc.* $\widetilde{v}^*_d$). These median $\widetilde{v}^*_d$ values were used to calculate the effective, deposition-corrected NH_3 recovered fractions (ξ_{NH3} and $\xi_{NH3/CH4}$) given in Table 4.

The median ξ_{NH3} (deposition-corrected) values derived from the line-integrated NH_3 concentration measurements were slightly larger than 1 (range 1.03 to 1.16; see Table 4). The highest deviation from 1 in the median value was calculated at the position closest to the surface, where model biases and model simplifications (in both dispersion and deposition) will be more pronounced compared to upper measurement heights. It remains unclear to what extent this seemingly systematic deviation from 1 was caused by either the deposition modeling or the imprecise CH_4 measurements by the GasFinder instruments (Section 2.2.1 and Häni et al., 2021). Nevertheless, a maximum deviation of only 16 % from the median value remains a promisingly small bias.

The NH_3 point concentration measurements showed ξ_{NH3} and $\xi_{NH3/CH4}$ values roughly at 0.9, whereas the vertical flux measurements

[2] Individual recovered fractions were assumed to approximately follow a log-normal distribution, since the uncertainty of the release rate from the source and the concentration measurement was expected to be small compared to the uncertainty in the modelled dispersion coefficient D which is inversely proportional to ξ (Fig. 13 in Supplement-1).

Table 2
Summary of estimated recovered fractions (ξ_{CH4} and ξ^0_{NH3}) without considering dry deposition of NH_3. meas. type: measured quantity being either concentration (conc) or vertical flux (flux). x_m: distance in meters between the source center and the center of the measurement. z_m: measurement height in meters above ground level. x_m / z_m: scaled fetch represented by the distance to the source divided by the measurement height. med: median recovered fraction. (lwr, upr): lower and upper bounds of the corresponding 95 %-CI for a single interval estimate (based on the log-transformed recovered fractions).

instrument type	meas. quantity	x_m	z_m	x_m / z_m	No. of intervals valid / total	Recovered fractions ξ^0	
						med	(lwr, upr)
CH_4							
line-integrated	conc	30	0.6	50	42 / 49	1.08	(0.83, 1.40)
			1.3	23	87 / 97	1.11	(0.92, 1.33)
		15	1.3	12	44 / 48	0.99	(0.74, 1.33)
		0	1.3	0	20 / 49	0.98	(0.62, 1.53)
point	conc	30	1.8	17	61 / 97	1.09	(0.63, 1.74)
	flux	30	1.8	17	55 / 97	0.96	(0.42, 2.21)
NH_3							
line-integrated	conc	30	0.6	50	67 / 75	0.65	(0.48, 0.87)
			1.3	23	66 / 75	0.64	(0.48, 0.86)
			2.1	14	25 / 29	0.66	(0.42, 1.02)
		15	1.3	12	24 / 26	0.72	(0.50, 1.02)
		0	1.3	0	24 / 49	0.71	(0.37, 1.37)
point	conc	30	1.8	17	31 / 49	0.53	(0.26, 1.09)
	flux	30	1.8	17	30 / 49	0.32	(0.17, 0.57)

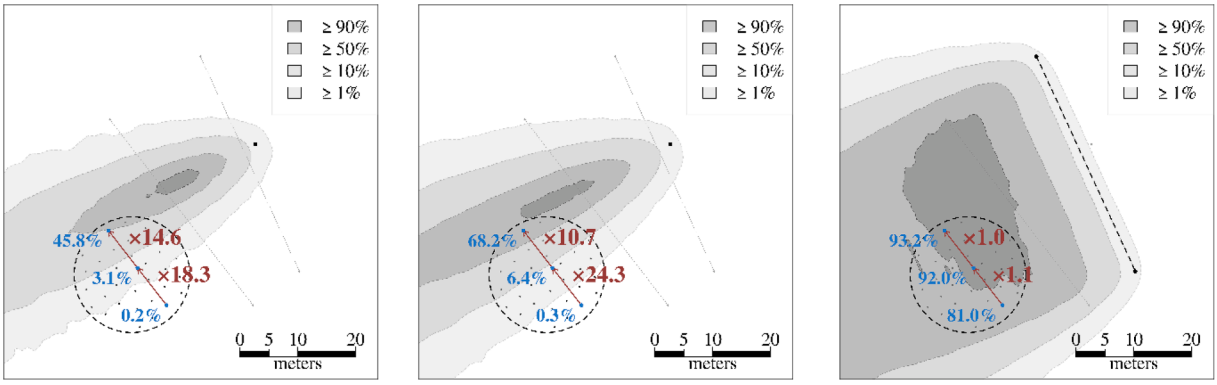

Fig. 2. Modelled footprint expressed as percentage (≥1 %, ≥10 %, ≥50 % and ≥90 %) of the footprint maximum for the flux (left), point concentration (middle) and the line-integrated concentration (right) measurements 30 m downwind of the source center. It should be noted that the generic term 'footprint' is used in the sense of 'footprint function' or 'source weight function' as discussed in Schmid (1994). The examples represent conditions as observed during experiment CH4-I on 2016-11-04 between 13:21 and 13:31. The single black dot and the two black dots connected by a dotted black line indicate the instrument positions in the northeast of the setup. The positions of the residual instruments are indicated in light gray. Blue dots represent three locations within the source area (indicated by a black, dashed circle) presented together with the corresponding source contribution (or source weight) values as percentage of the maximum. Red arrows and corresponding numbers indicate ratios between two neighboring locations.

showed significantly lower values around 0.6. Such lower ξ_{NH3} and $\xi_{NH3/CH4}$ values from the vertical flux measurements could be expected to some extent. Dry deposition related reductions differ for concentration and vertical flux measurements (Fig. 3c) since the flux footprint is smaller than the concentration footprint (see Fig. 2) and, therefore, the deposition flux between the source and the measurement location has a higher impact on the vertical flux measurement. However, the model results could not fully explain the observed underestimation of the flux-based NH_3 recovered fractions (Table 4; point flux) which remained systematically lower than the corresponding CH_4 recovered fractions even after deposition correction. It is likely that the applied ogive method to estimate the necessary high frequency damping correction of the NH_3 flux calculated by EC was too low (an average correction of 40 % was applied, where a correction of roughly 65 % would have been necessary to obtain a median recovered fraction of 1). Estimation of the high frequency damping correction for sticky compounds like NH_3 is not trivial and often leads to underestimation of the calculated flux values (Moravek et al., 2019 including the interactive comment SC1: https://amt.copernicus.org/preprints/amt-2019–193/amt-2019–193-SC1.pdf). This underestimation of the high frequency damping is mainly a problem of closed-path instruments (especially with significant lengths of inlet tubing), and is less an issue if open-path instruments are used for eddy covariance flux measurements (see Swart et al., 2023).

It should be noted that estimates of model deposition velocities $\widetilde{v}_d^*$ can be derived from recovered fractions only when emission rates are known, as in the case of release experiments. However, without a known emission rate, it is difficult to provide reasonably accurate values of v_d^* even when taking into account appropriate deposition pathways and parametrizations as discussed in Flechard et al. (2013). In cases where an accurate deposition velocity is not available, estimating and using an upper limit for it (as has been done e.g. in Valach et al., 2023) can help to constrain the model results and investigated source emissions (between zero and maximum deposition cases).

3.4. *Effect of deposition on modelled concentration and flux profiles*

All results presented in previous sections were performed for a source consisting of 36 small circular areas (Fig. 1), allowing NH_3 to deposit between the individual release orifices. This corresponds to the setup of our artificial grid source. However, in many emission source configurations (e.g. slurry tanks, plots of surface-spread slurry, etc.) there is a clear separation of emitting and depositing areas. For a general, systematic evaluation of the effect of deposition on concentration and flux

Table 3

Measurement-inferred surface deposition velocities ($\widetilde{v}_d^*$) for each measurement location and each release experiment, as well as the estimates of both the model surface ($\widetilde{v}_d^*$) and the 2 m height ($\widetilde{v}_d$) deposition velocity based on all concentration measurements (all units: cm s^{-1}). The values were derived from constraining $\xi_{NH3/CH4} = 1$. Values provided are the median ± a robust estimate of the standard deviation and the number of individual results (in parentheses) that the values are based on. x_m: distance in meters between the source center and the center of the measurement. z_m: measurement height in meters above ground level.

Meas. type	x_m	z_m	Surface deposition velocity ($\widetilde{v}_d^*$) in cm s^{-1}				
			Mix-I	Mix-II	Mix-III	Mix-IV	Mix-V
line-integrated conc.	30	0.6	n.a.	n.a.	n.a.	3.0 ± 0.7 (9)	1.7 ± 0.5 (8)
		1.3	4.1 ± 2.3 (7)	4.4 ± 0.6 (8)	6.3 ± 1.7 (9)	5.3 ± 1.3 (9)	2.0 ± 0.7 (7)
		2.1	n.a.	n.a.	n.a.	n.a.	n.a.
	15	1.3	3.1 ± 1.1 (7)	2.5 ± 0.5 (8)	2.9 ± 1.2 (8)	n.a.	n.a.
	0	1.3	n.a.	n.a.	n.a.	n.a.	2.2 ± 1.1 (6)
point conc.	30	1.8	n.a.	n.a.	n.a.	7.2 ± 3.4 (8)	3.1 ± 0.6 (3)
point flux	30	1.8	n.a.	n.a.	n.a.	13.1 ± 2.9 (9)	7.8 (1)
all conc.	$\widetilde{v}_d^*$		3.7 ± 1.3 (14)	3.6 ± 1.5 (16)	5.8 ± 3.1 (17)	5.1 ± 2.8 (26)	1.9 ± 0.9 (24)
	$\widetilde{v}_d$ @ 2m		0.8 ± 0.1 (14)	1.1 ± 0.2 (16)	1.6 ± 0.3 (17)	1.7 ± 0.3 (26)	0.7 ± 0.2 (24)

Meas. type	x_m	z_m	Surface deposition velocity ($\widetilde{v}_d^*$) in cm s^{-1}			
			Mix-VI	Mix-VII	Mix-VIII	Mix-IX
line-integrated conc.	30	0.6	3.6 ± 1.6 (12)	2.3 ± 0.4 (4)	1.3 ± 0.7 (7)	1.9 ± 0.7 (2)
		1.3	4.8 ± 2.8 (12)	3.7 ± 1.1 (4)	1.8 ± 0.6 (7)	2.8 ± 0.2 (2)
		2.1	n.a.	n.a.	n.a.	n.a.
	15	1.3	n.a.	n.a.	n.a.	n.a.
	0	1.3	6.4 ± 3.8 (5)	3.4 ± 2.0 (4)	2.0 ± 0.1 (3)	1.8 ± 0.1 (2)
point conc.	30	1.8	7.2 ± 4.1 (9)	3.7 ± 0.6 (2)	2.1 ± 1.7 (6)	5.6 (1)
point flux	30	1.8	7.1 ± 2.7 (8)	4.3 ± 4.9 (2)	6.0 ± 5.3 (5)	n.a.
all conc.	$\widetilde{v}_d^*$		4.6 ± 2.7 (38)	3.3 ± 1.3 (14)	1.7 ± 0.7 (23)	2.4 ± 0.9 (7)
	$\widetilde{v}_d$ @ 2m		1.3 ± 0.3 (38)	1.1 ± 0.4 (14)	0.6 ± 0.2 (23)	1.2 ± 0.3 (7)

measurements in various locations within the plume, we performed a series of standard model calculations based on neutral stability and median values of input variables as measured during the presented release experiments, given a contiguous source area with a radius of 10 m and a homogeneous emission rate over the entire area (allowing no deposition within this area).

Fig. 3a and b show the changes with height and distance of the emission-scaled concentration and vertical flux enhancements in the center of the emission plume and Fig. 3c shows the corresponding ratios of these quantities modelled with deposition divided by those modelled without deposition (details on modelled profiles for a grid source emission are given in Supplement-1 Fig. 22). Due to the limited source area, the dilution of the emission plume caused by dispersion is very efficient and both the concentrations and the vertical flux values decrease quickly with increasing distance independent of whether dry deposition has been included or not. The deposition-related reductions in the concentration and the flux dispersion factors differ significantly. Specifically for longer distances further downwind from the source, the emission-scaled fluxes show a much higher reduction due to dry deposition compared to the emission-scaled concentrations. Close to the ground, where the dry deposition takes place, values of the scaled fluxes become negative, reflecting that the deposition flux within the flux footprint contributes more to the net flux at the measurement location than the emission from the source.

Fig. 3d illustrates the total deposition (i.e., the cumulative loss due to deposition in the area between the source and the measurement location) downwind of the source in percentage of the total emission for both the single large source area used for the simulations in Fig. 3a-c as well as the source represented by 36 individual orifices. It is visible that a patchwork of distributed small emission areas can strongly increase the total dry deposition loss compared to a single large emission area, where deposition inside the source area itself is assumed to be zero. In the present experimental setup, the deposition to the circumference area of the release grid amounts to 27 % of the emission from the artificial source (difference between 36 orifices and circular area) at 30 m downwind which contributes to about 73.5 % of the total deposition. Both situations representing a single extended source or a distribution of point-like sources of NH_3 are found in the real world. The first case represents emission sources such as slurry tanks or broadcast manure spreading, while the latter applies for example to urine patches on a grazed pasture. If the short-range re-deposition on the pasture itself is not taken into account in the dispersion modeling, the obtained emission rate represents an effective net NH_3 emission of the pasture area (as done in Voglmeier et al., 2018).

It is evident that the total deposition up to a measurement location is not necessarily equal to the percentage reduction in the concentration

Table 4

Dry deposition-corrected recovered fractions of NH_3. x_m: distance in meters between the source center and the center of the measurement. z_m: measurement height in meters above ground level. N: number of valid results. med: median recovered fractions. (lwr, upr): lower and upper bounds of the corresponding 95 %-CI for a single interval estimate (based on the logarithmized recovered fractions).

tracer	meas. type	x_m	z_m	$\xi_{NH3/CH4}$			ξ_{NH3}		
				N	med	(lwr, upr)	N	med	(lwr, upr)
NH_3	line-integrated conc.	30	0.6	42	1.07	(0.88, 1.30)	67	1.16	(0.89, 1.51)
			1.3	65	0.95	(0.81, 1.12)	66	1.03	(0.85, 1.24)
			2.1	0	*n.a.*	*n.a.*	25	1.07	(0.74, 1.54)
		15	1.3	23	1.07	(0.92, 1.25)	24	1.07	(0.73, 1.58)
		0	1.3	20	0.98	(0.76, 1.28)	24	1.05	(0.57, 1.94)
	point conc.	30	1.8	29	0.90	(0.66, 1.24)	31	0.90	(0.52, 1.54)
	point flux	30	1.8	25	0.61	(0.21, 1.83)	30	0.57	(0.25, 1.29)

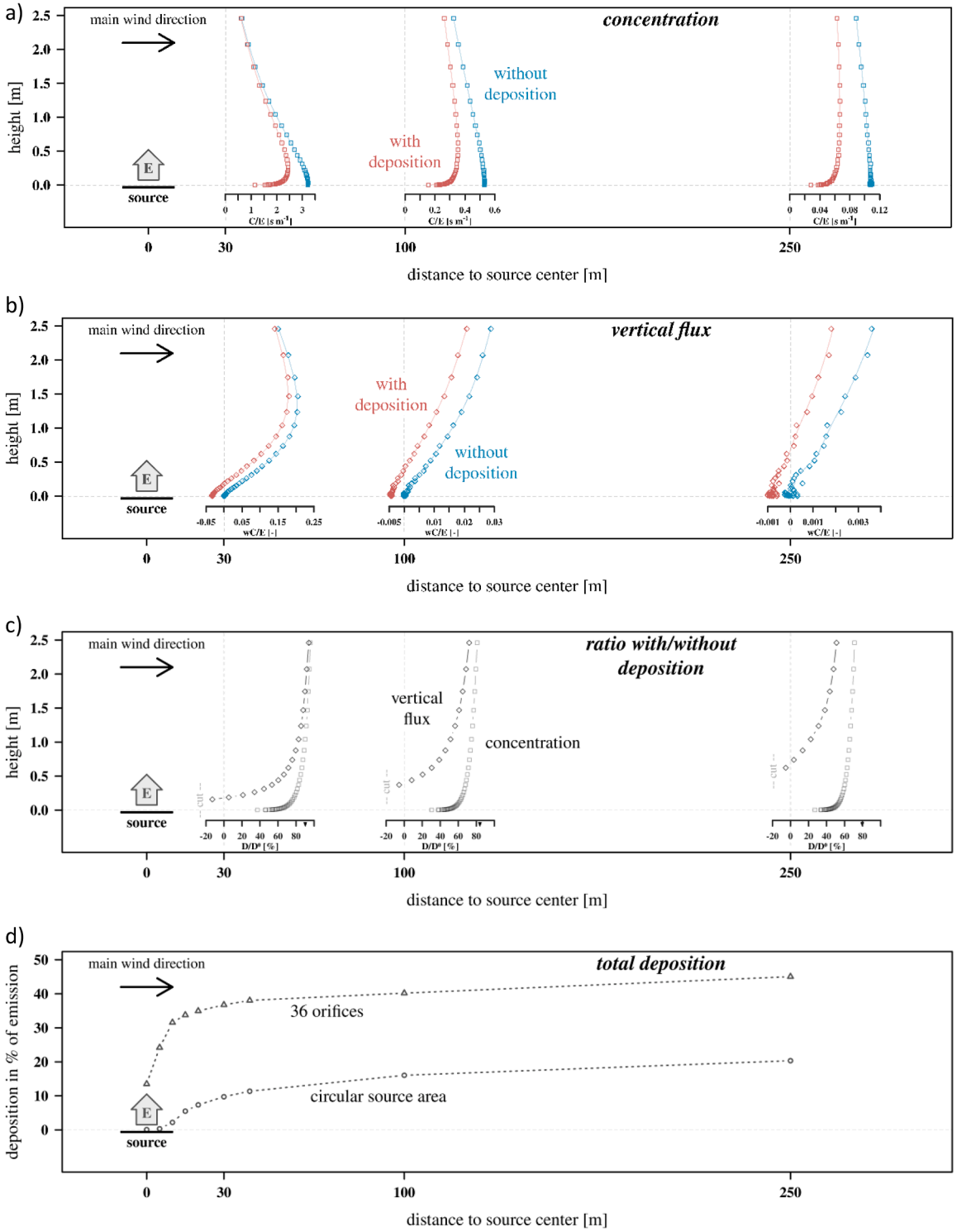

Fig. 3. Effect of deposition on modelled vertical profiles of emission-scaled concentration and flux enhancements in the center of an emission plume, and modelled total deposition as a function of distance downwind of a source. The model was run given neutral stability (L = -2000 m), $u_* = 0.25$ m s^{-1}, $z_0 = 0.3$ cm, $d = 4$ cm (for a canopy of 6 cm), $\sigma_u/u_* = \sigma_v/u_* = 3.3$, $\sigma_w/u_* = 1.2$, and a modelled surface deposition velocity of $v_d^* = 3$ cm s^{-1}. The examples are based on a circular area source with a radius of 10 m, which provides smoother profiles (i.e., with less modeling noise due to the large fraction of touchdowns inside the source area) and, therefore, are easier to interpret, in particular for distances beyond 30 m. Top to bottom: a) concentration to emission ratio (C / E) in s m^{-1} with (red) and without deposition (blue); b) vertical flux to emission ratio (wC / E) with and without deposition; c) ratios between dispersion factors with deposition and without deposition (D / D^0) given in percent (diamonds: vertical flux, squares: concentration); d) total deposition in percent of the total emission as a function of distance to the source from both source configurations, i.e., the circular source area with a radius of 10 m, as well as the 36 individual sources, each with a radius of 5 cm, as used to model the final recovered fractions.

and the vertical fluxes as already pointed out in Valach et al. (2023). Both depend on atmospheric and surface properties, as well as the distance to the source, but the reduction in the concentrations and fluxes depends on the footprint-weighted share of deposition between source and sensor, whereas the total deposition is independent of footprints. For example, at 30 m distance Fig. 3c shows a height-dependent reduction in concentration which ranges from roughly 10 to 60 % while the total deposition between the source and 30 m distance does not exceed 9.7 % (Fig. 3d).

4. Conclusion

For the presented experimental setup and data analysis, the bLS model provided emission rate estimates for the conserved tracer CH_4, which has negligible surface emission or uptake between source and the measurement locations, that agreed well with the actual release rates, independent of measurement locations or measurement conditions. The model performed exceptionally well if appropriate data quality assurance and selection was applied. A particularly important quality criterion was related to the wind direction where data was excluded when instruments were measuring at the edge of the plume and only marginally captured the trace gas plume. Flesch et al. (2004) already recommended to avoid such situations where the instruments measure near the plume edge. The reason for the low quality results at the plume edges lies in the high sensitivity of the dispersion factor on model input parameters such as wind direction, wind statistics etc., i.e., small biases in these input parameters result in large biases of the dispersion factor. This effect could also be seen with the measurements directly above the source, where the instrument path was most of the time at the plume edge too.

Line-integrating measurements with open-path instruments achieved more precise emission estimates compared to the point measurements with the closed-path instruments, which was related to the better coverage of the trace gas plume and less dependence on variations in the wind direction due to the longer measurement paths. This is only true if the precision and the accuracy of the concentration measurement is high. E.g., the use of the GasFinder sensors close to their sensitivity limit (e.g., in the case of measurements downwind of a small farm) can introduce significant biases in the concentration measurements (Häni et al., 2021). If the concentration measurements cannot be corrected as done in this study (Section 2.2.1), the emission estimates based thereon can be significantly biased, albeit given perfect plume coverage.

In the case of NH_3, surface dry deposition between the release and the measurement location was found to substantially reduce the measured concentration downwind of the source and NH_3 emissions were systematically underestimated by the bLS model without the inclusion of dry deposition removal. In general, assuming surface uptake occurs, measurement- and dispersion-based NH_3 emission estimates will be biased low if the effect of dry deposition loss is not taken into account in the data evaluation process; although one should also check if the underlying soil and vegetation emit NH_3, which may occur under dry and warm conditions in fertilized agro-ecosystems, even in so-called background situations (Flechard et al., 2010).

It is important to realize that both concentrations and vertical fluxes as measured by EC or the aerodynamic gradient method, always reflect the footprint-weighted summation of a spatial patchwork of different emission and deposition strengths. Reductions in the concentrations or vertical fluxes are not equal to the total amounts which are deposited between the source and sensors, since dry-deposition related reductions in the measured quantities (both concentration or vertical flux) are footprint-related and depend on measurement location and atmospheric conditions.

CRediT authorship contribution statement

Christoph Häni: Writing – original draft, Visualization, Methodology, Formal analysis, Data curation, Conceptualization. **Albrecht Neftel:** Writing – review & editing, Methodology. **Christophe Flechard:** Writing – review & editing, Methodology. **Christof Ammann:** Writing – review & editing, Methodology. **Alex Valach:** Writing – review & editing. **Thomas Kupper:** Writing – review & editing, Funding acquisition.

Declaration of competing interest

The authors declare that they have no known competing financial interests or personal relationships that could have appeared to influence the work reported in this paper.

Data availability

Data will be made available on request.

Acknowledgements

We thank Markus Jocher (Climate and Agriculture Group, Agroscope, Zürich) for the technical support and assistance during the release experiments. Funding has been provided by the Swiss Federal Office for the Environment (Contract 06.9115.P2l P263-1069).

Supplementary materials

Supplementary material associated with this article can be found, in the online version, at doi:10.1016/j.agrformet.2024.110041.

References

Ammann, C., Brunner, A., Spirig, C., Neftel, A., 2006. Technical note: water vapour concentration and flux measurements with PTR-MS. Atmos. Chem. Phys. 6 (12), 4643–4651.

Ammann, C., Jocher, M., Voglmeier, K., 2019. Eddy covariance flux measurements of NH 3 and NO y with a dual-channel thermal converter. In: *2019 IEEE International Workshop on Metrology for Agriculture and Forestry (MetroAgriFor). 2019 IEEE International Workshop on Metrology for Agriculture and Forestry (MetroAgriFor)*, Portici, Italy. 10/24/2019 - 10/26/2019. IEEE, pp. 46–51.

Ammann, C., Wolff, V., Marx, O., Brümmer, C., Neftel, A., 2012. Measuring the biosphere-atmosphere exchange of total reactive nitrogen by eddy covariance. Biogeosciences 9 (11), 4247–4261.

Bai, M., Suter, H., Lam, S.K., Sun, J., Chen, D., 2014. Use of open-path FTIR and inverse dispersion technique to quantify gaseous nitrogen loss from an intensive vegetable production site. Atmos. Environ. 94, 687–691.

Boreal Laser Inc., 2016. GasFinder3-OP Operation Manual. Part No. NDC-200029-D.

Bühler, M., Häni, C., Ammann, C., Mohn, J., Neftel, A., Schrade, S., Zähner, M., Zeyer, K., Brönnimann, S., Kupper, T., 2021. Assessment of the inverse dispersion method for the determination of methane emissions from a dairy housing. Agric. For. Meteorol. 307, 108501.

Coates, T.W., Alam, M., Flesch, T.K., Hernandez-Ramirez, G., 2021. Field testing two flux footprint models. Atmos. Meas. Tech. 14 (11), 7147–7152.

Coates, T.W., Flesch, T.K., McGinn, S.M., Charmley, E., Chen, D., 2017. Evaluating an eddy covariance technique to estimate point-source emissions and its potential application to grazing cattle. Agric. For. Meteorol. 234-235, 164–171.

Feitz, A., Schroder, I., Phillips, F., Coates, T., Negandhi, K., Day, S., Luhar, A., Bhatia, S., Edwards, G., Hrabar, S., Hernandez, E., Wood, B., Naylor, T., Kennedy, M., Hamilton, M., Hatch, M., Malos, J., Kochanek, M., Reid, P., Wilson, J., Deutscher, N., Zegelin, S., Vincent, R., White, S., Ong, C., George, S., Maas, P., Towner, S., Wokker, N., Griffith, D., 2018. The Ginninderra CH4 and CO2 release experiment: an evaluation of gas detection and quantification techniques. Int. J. Greenh. Gas Control 70, 202–224.

Flechard, C.R., Massad, R.S., Loubet, B., Personne, E., Simpson, D., Bash, J.O., Cooter, E. J., Nemitz, E., Sutton, M.A., 2013. Advances in understanding, models and parameterizations of biosphere-atmosphere ammonia exchange. Biogeosciences 10 (7), 5183–5225.

Flechard, C.R., Spirig, C., Neftel, A., Ammann, C., 2010. The annual ammonia budget of fertilised cut grassland – Part 2: seasonal variations and compensation point modeling. Biogeosciences 7 (2), 537–556.

Flesch, T.K., 1996. The footprint for flux measurements, from backward Lagrangian stochastic models. Bound.-Layer Meteor. 78 (3–4), 399–404.

Flesch, T.K., Wilson, J.D., Harper, L.A., Crenna, B.P., Sharpe, R.R., 2004. Deducing ground-to-air emissions from observed trace gas concentrations: a field trial. J. Appl. Meteorol. 43 (3), 487–502.

Flesch, T.K., Wilson, J.D., Yee, E., 1995. Backward-time lagrangian stochastic dispersion models and their application to estimate gaseous emissions. J. Appl. Meteorol. 34 (6), 1320–1332.
Häni, C., Bühler, M., Neftel, A., Ammann, C., Kupper, T., 2021. Performance of open-path GasFinder3 devices for CH_4 concentration measurements close to ambient levels. Atmos. Meas. Tech. 14 (2), 1733–1741.
Häni, C., Flechard, C., Neftel, A., Sintermann, J., Kupper, T., 2018. Accounting for field-scale dry deposition in backward lagrangian stochastic dispersion modelling of NH3 emissions. Atmosphere 9 (4), 146.
Harper, L.A., Flesch, T.K., Weaver, K.H., Wilson, J.D., 2010. The effect of biofuel production on swine farm methane and ammonia emissions. J. Environ. Qual. 39 (6), 1984–1992.
Hu, N., Flesch, T.K., Wilson, J.D., Baron, V.S., Basarab, J.A., 2016. Refining an inverse dispersion method to quantify gas sources on rolling terrain. Agric. For. Meteorol. 225, 1–7.
Lavrsen Kure, J., Krabben, J., Vilms Pedersen, S., Carozzi, M., Sommer, S., 2018. An assessment of low-cost techniques to measure ammonia emission from multi-plots: a case study with urea fertilization. Agronomy 8 (11), 245.
Lemes, Y.M., Nyord, T., Feilberg, A., Kamp, J.N., 2023. Effect of covering deep litter stockpiles on methane and ammonia emissions analyzed by an inverse dispersion method. ACS Agric. Sci. Technol. 3 (5), 399–412.
Leytem, A.B., Dungan, R.S., Bjorneberg, D.L., Koehn, A.C., 2011. Emissions of ammonia, methane, carbon dioxide, and nitrous oxide from dairy cattle housing and manure management systems. J. Environ. Qual. 40 (5), 1383–1394.
Loubet, B., Asman, W.A.H., Theobald, M.R., Hertel, O., Tang, Y.S., Robin, P., Hassouna, M., Dämmgen, U., Genermont, S., Cellier, P., Sutton, M.A., 2009. Ammonia deposition near hot spots: processes, models and monitoring methods. In: Sutton, M.A., Reis, S., Baker, S.M. (Eds.), Atmospheric Ammonia. Springer Netherlands, Dordrecht, pp. 205–267.
McGinn, S.M., Coates, T., Flesch, T.K., Crenna, B., 2008. Ammonia emission from dairy cow manure stored in a lagoon over summer. Can. J. Soil Sci. 88 (4), 611–615.
Moravek, A., Singh, S., Pattey, E., Pelletier, L., Murphy, J.G., 2019. Measurements and quality control of ammonia eddy covariance fluxes: a new strategy for high-frequency attenuation correction. Atmos. Meas. Tech. 12 (11), 6059–6078.
Nemitz, E., Dorsey, J.R., Flynn, M.J., Gallagher, M.W., Hensen, A., Erisman, J.W., Owen, S.M., Dämmgen, U., Sutton, M.A., 2009. Aerosol fluxes and particle growth above managed grassland. Biogeosciences 6 (8), 1627–1645.
Ro, K.S., Johnson, M.H., Stone, K.C., Hunt, P.G., Flesch, T., Todd, R.W., 2013. Measuring gas emissions from animal waste lagoons with an inverse-dispersion technique. Atmos. Environ. 66, 101–106.
Schmid, H.P., 1994. Source areas for scalars and scalar fluxes. Bound.-Layer Meteor. 67 (3), 293–318.
Schrader, F., Brümmer, C., 2014. Land use specific ammonia deposition velocities: a review of recent studies (2004-2013). Water Air Soil Pollut. 225 (10), 2114.
Shonkwiler, K.B., Ham, J.M., 2018. Ammonia emissions from a beef feedlot: comparison of inverse modeling techniques using long-path and point measurements of fenceline NH3: comparison of inverse modeling techniques using long-path and point measurements of fenceline NH 3. Agric. For. Meteorol. 258, 29–42.
Sintermann, J., Ammann, C., Kuhn, U., Spirig, C., Hirschberger, R., Gärtner, A., Neftel, A., 2011. Determination of field scale ammonia emissions for common slurry spreading practice with two independent methods. Atmos. Meas. Tech. 4 (9), 1821–1840.
Sintermann, J., Dietrich, K., Häni, C., Bell, M., Jocher, M., Neftel, A., 2016. A miniDOAS instrument optimised for ammonia field measurements. Atmos. Meas. Tech. 9 (6), 2721–2734.
Swart, D., Zhang, J., van der Graaf, S., Rutledge-Jonker, S., Hensen, A., Berkhout, S., Wintjen, P., van der Hoff, R., Haaima, M., Frumau, A., van den Bulk, P., Schulte, R., van Zanten, M., van Goethem, T., 2023. Field comparison of two novel open-path instruments that measure dry deposition and emission of ammonia using flux-gradient and eddy covariance methods. Atmos. Meas. Tech. 16 (2), 529–546.
Valach, A.C., Häni, C., Bühler, M., Mohn, J., Schrade, S., Kupper, T., 2023. Ammonia emissions from a dairy housing and wastewater treatment plant quantified with an inverse dispersion method accounting for deposition loss. J. Air. Waste. Manag. Assoc.
Voglmeier, K., Jocher, M., Häni, C., Ammann, C., 2018. Ammonia emission measurements of an intensively grazed pasture. Biogeosci. Discuss 1–32.
Wang, W., Liu, W., Zhang, T., Lu, Y., 2014. Measuring greenhouse-gas emissions from a synthetic tracer source. J. Appl. Spectrosc. 81 (2), 264–272.
Wintjen, P., Ammann, C., Schrader, F., Brümmer, C., 2020. Correcting high-frequency losses of reactive nitrogen flux measurements. Atmos. Meas. Tech. 13 (6), 2923–2948.
Yang, W., Zhu, A., Zhang, J., Zhang, X., Che, W., 2016. Assessing the backward Lagrangian stochastic model for determining ammonia emissions using a synthetic source. Agric. For. Meteorol. 216, 13–19.